COVER SHEET

Title: Enhanced Damage Detection in Conductive Polymer-based Composites through Piezoresistive Coupling

Authors: Tyler Tallman
Fabio Semperlotti
Kon-Well Wang

ABSTRACT

Because of its ability to spatially resolve damage without invasive measurements, electrical impedance tomography (EIT) has tremendous potential for the health monitoring of nanocomposites wherein networks of nanofillers impart conductive properties to an otherwise insulating matrix. Matrix cracking will sever the conductive network thereby manifesting as abrupt, local changes in conductivity. However, EIT is insensitive to abrupt, local changes in conductivity. Furthermore, experimental EIT requires a burdensome number of sensors. This paper explores how the piezoresistivity of nanocomposites can be exploited to enhance the sensitivity of EIT to abrupt, local changes in conductivity while decreasing its sensor requirements.

INTRODUCTION

Fibrous composites are increasingly prevalent structural materials due to their high strength-to-weight ratio, but their laminar construction makes them susceptible to delamination. Delamination is preceded by matrix cracking which can be initiated through manufacturing defects, fastening and joining, critical geometry configurations, and low velocity impacts [1]. Accurate and expedient matrix monitoring remains a crucial yet challenging aspect of structural identification in fibrous composites.

Composites manufactured with carbon nanotube (CNT) or carbon nanofibers (CNF) fillers have demonstrated potential for damage detection [2] [3] [4], strain sensing [5] [6] [7] [8] [9], and damping enhancement [10] [11] [12]. The conductivity of nanocomposites depends upon the formation of a well dispersed and

Tyler Tallman and Kon-Well Wang, University of Michigan Department of Mechanical Engineering, 2350 Hayward Street, Ann Arbor, MI, USA 48109-2125.
Fabio Semperlotti, University of Notre Dame Department of Aerospace and Mechanical Engineering, 374 Fitzpatrick Hall of Engineering, South Bend, IN, USA 46556-5637.

connected network of nanofillers within a matrix material. Any mechanical perturbation which changes network parameters such as filler orientation or inter-filler spacing will change the composite's conductivity. The dependence of electrical diffusive properties on mechanical state is known as piezoresistivity [13]. Matrix cracking will sever the connection between neighboring fillers. This will create a region of greatly reduced conductivity the location of which coincides with the damage. Therefore, monitoring the conductivity of nanocomposites offers insight into their damage state.

Recently, EIT has received excellent treatment as a health monitoring technique for nanocomposites [5] [6] and cementitious structures [14]. EIT images the internal conductivity distribution of a structure using periphery current injections and voltage measurements. However, mathematically, EIT is a highly rank deficient inverse problem whose regularization gives preference to smeared or distorted conductivity distributions. If the conductivity change due to matrix cracking is small enough, this smearing makes the damage indistinguishable from the background conductivity. Furthermore, accurate EIT images typically require from sixteen to thirty-two sensing electrodes. An ideal health monitoring scheme should be easily implementable, but it is difficult to discern damage if too few electrodes are used. This research explores the influence of incorporating globally known conductivity changes into the EIT imaging technique to increase sensitivity to abrupt, local conductivity changes while minimizing the number of electrodes to capture damage. While it is possible to predict global conductivity changes of arbitrarily strained domains [13], we restrict our attention to artificially imposed conductivity changes on two-dimensional domains.

ELECTRICAL IMPEDANCE TOMOGRAPHY FORMULATION

EIT maps the internal conductivity distribution of a structure by minimizing the difference between a forward operator which predicts electrode voltages as they depend upon the internal conductivity and experimentally measured voltages in an augmented least-squares sense via a Newton-Raphson method [15].

$$min\left(\|\boldsymbol{V}_m - \boldsymbol{F}(\sigma)\|^2 + \boldsymbol{G}(\sigma)\right) \tag{1}$$

Where $\boldsymbol{V}_m$ is a vector of measured boundary voltages, $\boldsymbol{F}(\sigma)$ is a vector of boundary voltages calculated by the forward operator for an estimated conductivity distribution σ, and $\boldsymbol{G}(\sigma)$ is a penalty function to regularize the minimization. This minimization process seeks to recover the conductivity coefficients of Kirchhoff's law for conduction within a continuum given by:

$$\boldsymbol{\nabla} \cdot \sigma \boldsymbol{\nabla} \phi = 0. \tag{2}$$

And subject to the complete electrode model boundary conditions:

$$\sigma \boldsymbol{\nabla} \phi \cdot \boldsymbol{n} = \frac{1}{z_l}(V_l - \phi), \tag{3}$$

$$\int \sigma \nabla \phi \cdot \boldsymbol{n} \partial \Omega = 0. \tag{4}$$

Where ϕ is the domain electric potential, $\boldsymbol{n}$ is an outward pointing normal, z_l is the contact impedance between the lth electrode and the domain, and V_l is the voltage on the lth electrode.

The forward problem is most expediently solved by finite elements where the conductivity coefficient in equation (1) now becomes a vector of unknowns, and EIT seeks to recover the conductivity of each element. Treated in more detail in [15], the forward problem is discretized in the following manner:

$$\begin{bmatrix} A_M + A_Z & A_W \\ A_W^T & A_D \end{bmatrix} \begin{bmatrix} \Phi \\ V \end{bmatrix} = \begin{bmatrix} 0 \\ I \end{bmatrix}, \tag{5}$$

$$A_{Z\,ij} = \sum_{l=1}^{L} \int_{E_l} \frac{1}{z_l} w_i w_j dS, \tag{6}$$

$$A_{W\,li} = -\frac{1}{z_l} \int_{E_l} w_i dS, \tag{7}$$

$$A_D = diag\left(\frac{|E_l|}{z_l}\right). \tag{8}$$

A_M is the standard diffusion stiffness matrix, Φ is a vector of the domain potentials, V is a vector of the electrode voltages, I is a vector of the current injections applied to electrode pairs (i.e. the first injection pattern could be specified as $I = [1 \quad -1 \quad 0 \quad \cdots \quad 0]^T$), E_l is the electrode area in three-dimensions or electrode length in two-dimensions, and w_i are the finite element interpolation functions. The solution to equation (5) is determined only up to an arbitrary constant voltage which is remedied by enforcing that the sum of the electrode voltages to be zero.

The conductivity distribution is recovered by first supplying a conductivity vector estimate and then iterating upon it to minimize a voltage error vector. Retaining only the linear terms of a Taylor series expansion, the minimization routine takes the following form:

$$\boldsymbol{V}_m - \boldsymbol{F}(\boldsymbol{\sigma}) - \frac{\partial \boldsymbol{F}(\boldsymbol{\sigma})}{\partial \boldsymbol{\sigma}} \boldsymbol{\Delta\sigma} = \boldsymbol{0}, \tag{9}$$

$$\boldsymbol{J\Delta\sigma} = \boldsymbol{V}_e. \tag{10}$$

Denoting the partial derivative of the forward operator with respect to the conductivity vector as the sensitivity matrix or $\boldsymbol{J}$ and the difference between the forward operator voltage vector and the measured voltage vector as $\boldsymbol{V}_e = \boldsymbol{F}(\boldsymbol{\sigma}) - \boldsymbol{V}_m$, equation (9) takes the form of equation (10). Ideally, the conductivity update could be recovered as $\boldsymbol{\Delta\sigma} = (\boldsymbol{J}^T\boldsymbol{J})^{-1}\boldsymbol{J}^T\boldsymbol{V}_e$, but $\boldsymbol{J}$ is severely rank deficient requiring the penalty function in equation (1) to eliminate non-physical solutions. The explicit solution to equation (1) follows from Tikhonov regularization, and the conductivity update takes the following form:

$$\boldsymbol{\Delta\sigma} = (\boldsymbol{J}^T\boldsymbol{J} + \alpha^2\boldsymbol{L}^T\boldsymbol{L})^{-1}\boldsymbol{J}^T\boldsymbol{V}_e. \tag{11}$$

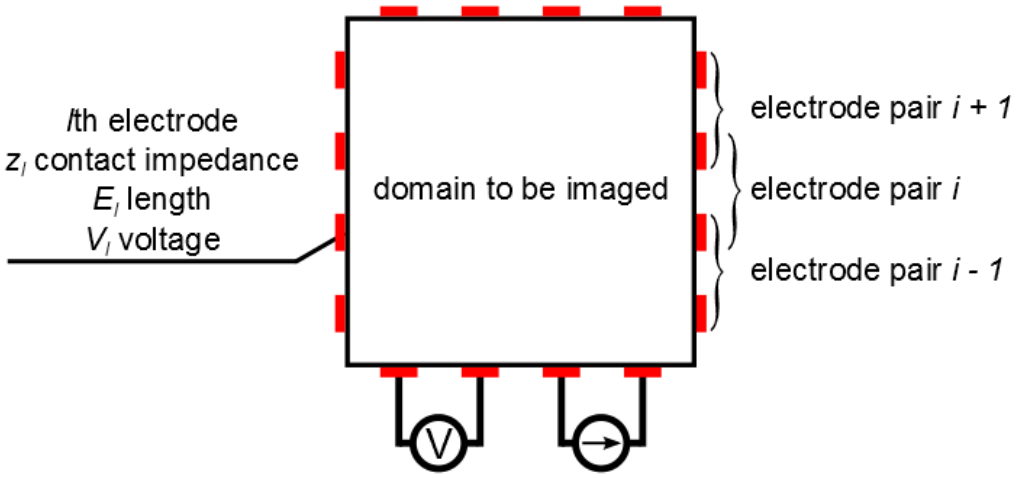

Figure 1. Schematic of EIT setup. Current is injected and voltage is measured between neighboring electrode pairs.

There are many clever approaches to selecting $\boldsymbol{L}$ (refer to [15]), but a common choice is $\boldsymbol{L}^T\boldsymbol{L} = \boldsymbol{I}$ where $\boldsymbol{I}$ is the identity matrix. However, voltage measurements are least sensitive to changes of conductivity on interior elements. This typically results in boundary elements undergoing large fluctuations in conductivity during the reconstruction process. In order to counter this, we employ a regularization technique which is larger for elements further removed from the center of the domain thereby adding greater penalty to their fluctuation. This can be expressed by making $\boldsymbol{L}^T\boldsymbol{L}$ a diagonal matrix with off-diagonal terms set to zero and diagonal terms set to $1 + r_e$ where r_e is the distance from the center of the domain to the centroid of the *e*th element. Lastly, the sensitivity matrix is formed in a manner not unlike the diffusion stiffness matrix as follows:

$$J_{\boldsymbol{ij\,k}} = \frac{\partial V_{ij}}{\partial \sigma_k} = -\int_{\Omega_k} \boldsymbol{\nabla}\phi_i \cdot \boldsymbol{\nabla}\phi_{\boldsymbol{j}} dV. \tag{12}$$

Here, *ij* is a single index of $\boldsymbol{J}$ and refers to the integral of the inner product between the gradient of the voltage due to the injection at the *i*th electrode pair and the gradient of the voltage due to the unit current injection between the *j*th electrode measurement pair. The *k* index refers to the element over which the integral is evaluated.

INCORPORATING GLOBAL CONDUCTIVITY CHANGES

Understanding the relationship between strain and conductivity of nanofiller networks is an active area of research [7] [8] [16] [17]. Recently, a method of predicting conductivity changes at every point of a domain subjected to arbitrary strains as a function of filler volume fraction, critical volume fraction, inter-filler spacing, and principals strains has been developed [13]. The ability to model global

conductivity changes due to strain motivates our method to enhance EIT through strain coupling. We endeavor to address the rank deficiency of the aforementioned sensitivity matrix by incorporating known conductivity changes.

To assess the validity of incorporating known conductivity changes into EIT imaging, we consider artificial conductivity changes that do not represent physical strains. However, for convenience, we will refer to a globally imposed, artificial conductivity change as a strain field. Let the changed conductivity vector be denoted as $\hat{\boldsymbol{\sigma}}$ and be related to the unchanged conductivity vector as

$$\hat{\boldsymbol{\sigma}} = \boldsymbol{G}\boldsymbol{\sigma}. \tag{13}$$

The artificial conductivity change we impose on the eth element takes the form:

$$\hat{\sigma}^e = \sigma_0 - \frac{\sigma_0}{2}\left(\sin\left(\frac{m\pi x_c^e}{L}\right)\sin\left(\frac{n\pi y_c^e}{H}\right)\right). \tag{14}$$

Where σ_0 is the initial conductivity estimate, x_c^e and y_c^e are the coordinates of the centroid of the eth element, and L and H are the length and height of the rectangular domain which is being imaged. The integer values m and n are the same for every element but change for different strain fields. This makes $\boldsymbol{G}$ a diagonal matrix of dimension equal to the number of elements with diagonal entries given by equation (14). Figure (2) provides an example of two different strain fields. Following the development of equations (9) and (10) but with $\hat{\boldsymbol{\sigma}}$, the following can be expressed:

$$\hat{\boldsymbol{J}}\boldsymbol{\Delta}\hat{\boldsymbol{\sigma}} = \hat{\boldsymbol{V}}_e. \tag{15}$$

The imposition of a strain field results in a new sensitivity matrix, voltage error vector, and change in conductivity to be recovered. However, in light of equation (13), this can be recast as

$$\hat{\boldsymbol{J}}\boldsymbol{G}\boldsymbol{\Delta}\boldsymbol{\sigma} = \hat{\boldsymbol{V}}_e. \tag{16}$$

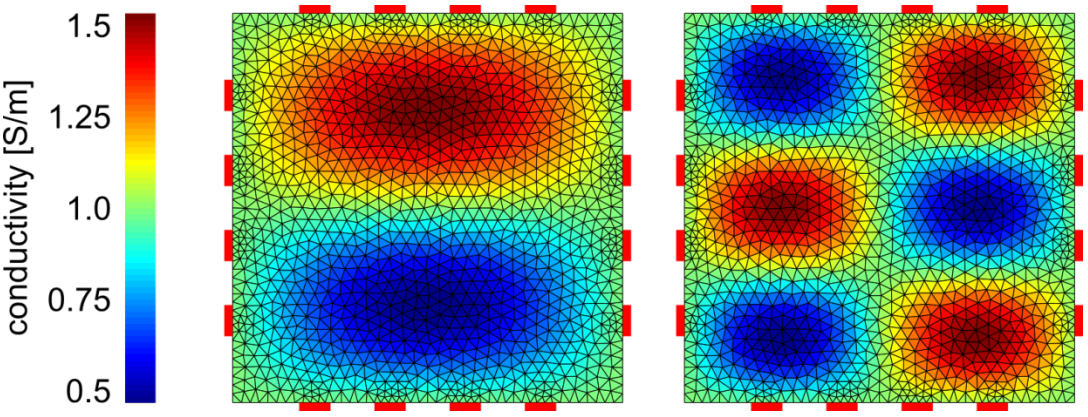

Figure 2. Two representative strain fields with the underlying reconstruction mesh are shown, m = 1 and n = 2 on the left while m = 2 and n = 3 on the right. Electrodes are shown along the periphery. The reference conductivity is 1 S/m.

The same change in conductivity vector is now to be solved for in both equations (10) and (16). This process can be repeated for arbitrarily many strain fields resulting in the following expression:

$$\begin{bmatrix} \boldsymbol{J} \\ \vdots \\ \hat{\boldsymbol{J}}^n \boldsymbol{G}^n \end{bmatrix} \boldsymbol{\Delta\sigma} = \begin{bmatrix} \boldsymbol{V}_e \\ \vdots \\ \hat{\boldsymbol{V}}_e^n \end{bmatrix}. \tag{17}$$

Superscripts in equation (17) refer to the *n*th strain field. The augmented sensitivity matrix can be inverted and the conductivity change vector recovered by again employing Tikhonov regularization.

ENHANCED DAMAGE IDENTIFICATION WITH STRAIN COUPLING

In lieu of experimental data, we test our method by reconstructing a damaged reference finite element mesh. Employing reference meshes is common practice in developing EIT routines, and, to avoid pitfalls associated with EIT development, the reference mesh is more refined (~3000 elements) than the reconstruction mesh (~2000 elements). Furthermore, we set $\alpha^2 = 1.0e^{-5}$ for every simulation. Adjusting α^2 from simulation to simulation during the developmental stage to obtain optimal results is considered poor practice since in experimental settings the optimal solution is unknown [15]. Damage is simulated by making the reference mesh a multiply connected domain as shown in figure (3). Lastly, we use a reference or undamaged conductivity value of $\sigma_0 = 1.0\, S/m$, constant contact impedance of $z_l = 1000\ \Omega m^2$, and unit current injections.

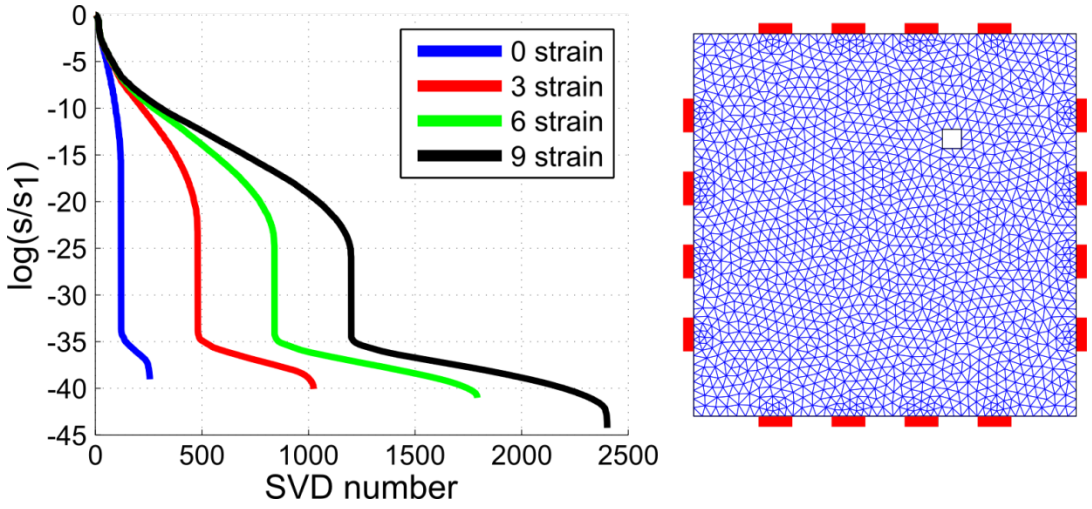

Figure 3. Left: SVD plots comparing the rank deficiency of the sensitivity matrices at zero, three, six, and nine strains for sixteen electrodes. Right: Reference finite element mesh.

Singular value decomposition (SVD) can be employed to assess the rank of the sensitivity matrices by plotting the natural logarithm of the singular values normalized by the first singular value of the sensitivity matrix against singular value number. The rank of the sensitivity matrix corresponds to the singular number at which the log of the normalized singular values drops suddenly. The singular values for the sixteen electrode scheme with zero, three, six, and nine strain fields are plotted in figure (3).

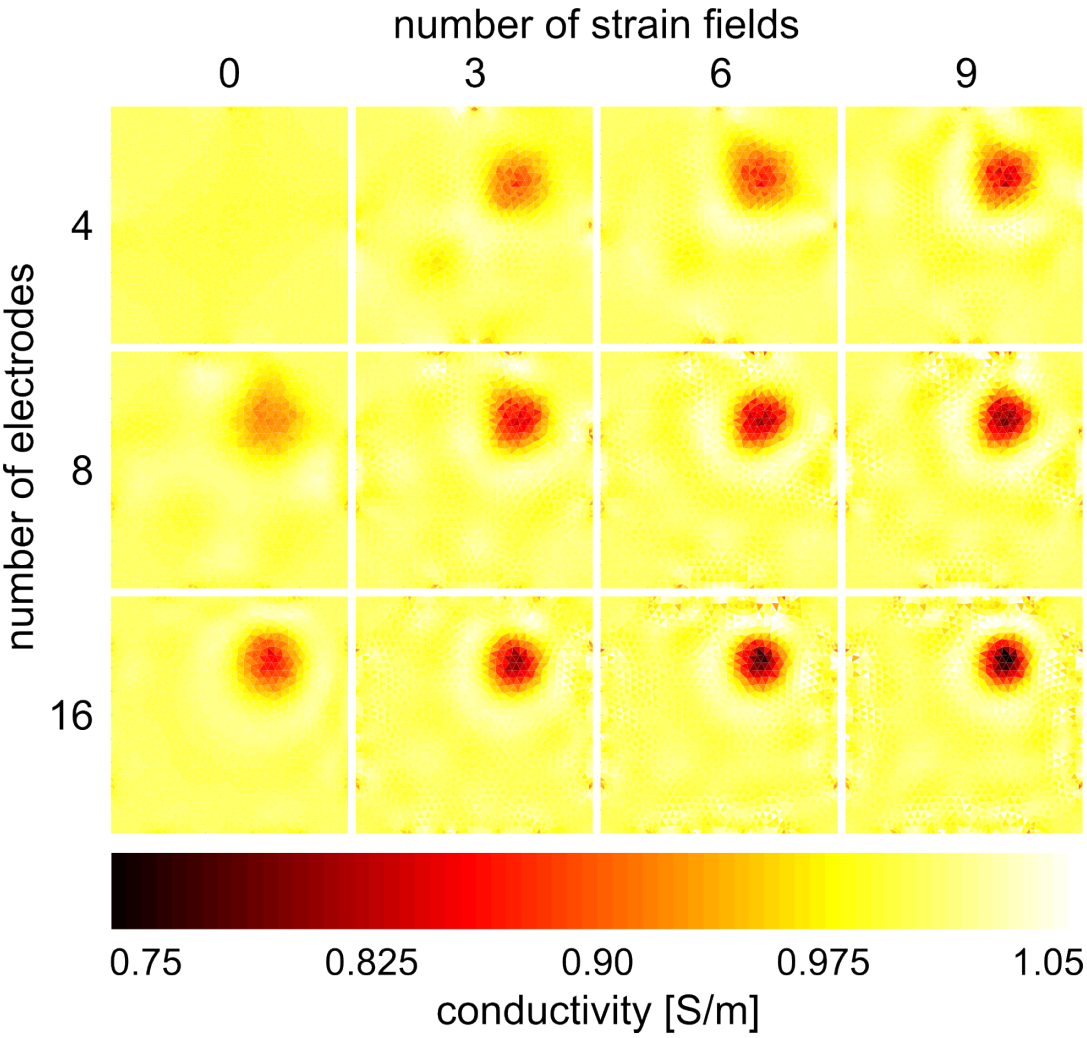

Figure 4. Comparison of damage detection with varying strain fields and electrodes. These results indicate that both the damage localization and clarity improve as the number of strain fields increases for any specified number of electrodes.

SUMMARY AND CONCLUSIONS

We have developed a method of enhancing damage identification via EIT by incorporating global conductivity changes such as those achievable through piezoresistive nanocomposites. Figure (4) shows that for any number of electrodes,

better images are obtained as the number of strain fields incorporated increases. Furthermore, we note that damage can be identified using as few as four electrodes with the addition of as few as three strain fields. Using four electrodes and nine strain fields produces images on par with a sixteen electrode scheme with no strains. As noted in the introduction, an important limitation of EIT in health monitoring is its cumbersome experimental setup which depends upon many electrodes for accurate imaging. We have shown that this limitation can be circumvented by addressing the rank deficiency of the sensitivity matrix through strain coupling.

ACKNOWLEDGEMENTS

This research is supported by the U.S. Army Research Office (W911NF-10-1-00267).

REFERENCES

1. Abrate, S. 2011. *Impact Engineering of Composite Structures*. CISM, pp. 108.
2. Böger, L., M. H. G. Winchmann, L. O. Meyer, and K. Schulte. 2008. "Load and Health Monitoring in Glass Fibre Reinforced Composites with an Electrically Conductive Nanocomposite Epoxy Matrix," Composites Science and Technology, 68(7 – 8): 1886 – 1894.
3. Nofar, M., S. V. Hoa, and M. D. Pugh. 2009. "Failure Detection and Monitoring in Polymer Matrix Composites Subjected to Static and Dynamic Loads using Carbon Nanotube Networks," Composites Science and Technology, 69(10): 1599 – 1606.
4. Thostenson, E. T. and T. W. Chou. 2008. "Real-Time in situ Sensing of Damage Evolution in Advanced Fiber Composites using Carbon Nanotube Networks," Nanotechnology, 19(21): 215713.
5. Hou, T.C., K. J. Loh, and J. P. Lynch. 2007. "Spatial Conductivity Mapping of Carbon Nanotube Composite Thin Films by Electrical Impedance Tomography for Sensing Applications," Nanotechnology, 18(31): 315501.
6. Loh, K. J., T. C. Hou, J. P. Lynch, and N. A. Kotov. 2009. "Carbon Nanotube Sensing Skins for Spatial Strain and Impact Damage Identification," Journal of Nondestructive Evaluation, 28(1): 9 – 25.
7. Hu, N., Y. Karube, M. Arai, T. Watanabe, C. Yan, and Y. Li. 2010. "Investigation on Sensitivity of a Polymer/Carbon Nanotube Composite Strain Sensor," Carbon, 48(3): 680 – 687.
8. Hu, N., Y. Karube, C. Yan, Z. Masuda, and H. Fukunaga. 2008. "Tunneling Effect in a Polymer/Carbon Nanotube Nanocomposite Strain Sensor," Acta Materialia, 56(13): 2929 – 2936.
9. Zhang, W., J. Suhr, and N. Koratkar. 2006. "Carbon Nanotube/Polycarbonate Composites as Multifunctional Strain Sensors," Journal of Nanoscience and Nanotechnology, 6(4): 960 – 964.
10. Zhou, X., E. Shin, K. W. Wang, and C. E. Bakis. 2004. "Interfacial Damping Characteristics of Carbon Nanotube-Based Composites," Composites Science and Technology, 64(15): 2425 – 2437.
11. Liu, A., K. W. Wang, and C. E. Bakis. 2011. "Effect of Functionalization of Single-Wall Carbon Nanotubes (SWNTs) on the Damping Characteristics of SWNT-Based Epoxy Composites via Multiscale Analysis," Composites A, 42(11): 1748 – 1755.

12. Liu, A., K. W. Wang, and C. E. Bakis. 2010. “Multiscale Damping Model for Polymeric Composites Containing Carbon Nanotube Ropes,” Journal of Composite Materials, 44(19): 2301 – 2323.
13. Tallman, T. and K. W. Wang. 2013. “An Arbitrary Strains Carbon Nanotube Composite Piezoresistivity Model for Finite Element Integration,” Applied Physics Letters, 102(1): 011909.
14. Hou, T. C. and J. P. Lynch. 2009. “Electrical Impedance Tomographic Methods for Sensing Strain Fields and Crack Damage in Cementitious Structures,” Journal of Intelligent Material Systems and Structures, 20(11): 1363 – 1379.
15. Lionheart, W. 2005. “The Reconstruction Problem,” in *Electrical Impedance Tomography: Methods, History, and Applications*, D. Holder, editor. London: Institute of Physics, pp. 3 – 62.
16. Hu, N., Z. Masuda, G. Yamamoto, H. Fukunaga, T. Hashida, and J. Qiu. 2008. “Effect of Fabrication Process on Electrical Properties of Polymer/Multi-Wall Carbon Nanotube Nanocomposites,” Composites A, 39(5): 893 – 903.
17. Rahman, R. and P. Servati. 2012. “Effects of Inter-Tube Distance and Alignment on Tunneling Resistance and Strain Sensitivity of Nanotube/Polymer Composite Films,” Nanotechnology, 23(5): 055703.